p-ISSN 2089 – 0133 e-ISSN 2477-6416
URL: https://jurnal.uns.ac.id/ijap/article/view/87415

DOI: https://doi.org/10.13057/ijap.v15i1.87415

USING FTIR ANALYSIS TO INVESTIGATE THE MINERALOGICAL COMPOSITION OF ULTISOLS AND ALFISOL IN SOUTHEAST EAST SULAWESI, INDONESIA

Rosliana Eso*[1], Tufaila[2], Arman[3]
[1]Departement of Physics Education, Halu Oleo University, Kendari, Indonesia
[2]Department of Soil Science, Halu Oleo University, Kendari, Indonesia
[3]Department of Mathematics, Halu Oleo University, Kendari, Indonesia
*rosliana.eso@uho.ac.id

Received 01-06-2024, Revised 28-02-2025, Accepted 01-04-2025,
Available Online 01-04-2025, Published Regularly April 2025

ABSTRACT

This study aims to investigate the mineralogical composition of Ultisols and Alfisols using the X-ray diffraction (XRD) analytical technique and FTIR analysis to provide fundamental information on these soil types. Thirty samples of Ultisols and Alfisols were collected from six selected sites with different profiles (i.e., Profile 1, Profile 2, and Profile 3) where these soils occur on limestone parent material. We used the Kjeldahl method to determine total nitrogen, a soil pH meter to measure pH, and the X-ray fluorescence (XRF) method to analyze chemical elements. Additionally, XRD in conjunction with FTIR spectroscopy was used to examine the mineralogical composition of both soil types.The average total nitrogen content across all profiles ranged from 0.1% to 0.35% for Ultisols and from 0.1% to 0.92% for Alfisols. The soil pH indicated an alkaline reaction, ranging from 4.5 to 5.3 for Ultisols and from 4.8 to 6.2 for Alfisols. Chemical element content obtained from oxides in all profiles included Si, Al, Fe, Mg, Ti, Ca, S, Na, K, P, Mn, Ni, Co, and Cr. Dominant Si trends, consistently increasing upward on both Ultisol and Alfisol sites, indicated significant soil development in the study area. The diffraction pattern graphics of topsoil from all profiles identified a 100% Silicon oxide quartz low (SiO2) phase with the trigonal (hexagonal axes) crystal system. FTIR spectroscopy analysis showed progressive kaolinization in all Alfisol samples. In contrast, Ultisol Profile 1 expressed montmorillonite, while Profiles 2 and 3 attributed to kaolinite. FTIR results consistently provided more accurate mineral analysis of Ultisol and Alfisol formations compared to XRD.

Keywords: Ultisol; Alfisol; FTIR Analysis; XRD Analysis; Mineral.

Cite this as: Eso, R., Tufaila., & Arman. 2025. Using FTIR Analysis to Investigate the Mineralogical Composition of Ultisols and Alfisol in Southeast East Sulawesi, Indonesia. *IJAP: Indonesian Journal of Applied Physics, 15*(1), 84-97. doi: https://doi.org/10.13057/ijap.v15i1.87415

INTRODUCTION

For a long time, various combinations of techniques for predicting soil properties related to soil fertility and mineral content in soils have been applied to evaluate soil mineralogical variations. XRD spectra and infrared spectroscopy (FTIR) are the tools usually used to capture vital mineralogical differences in soils associated with different soil types. Transmission FTIR spectroscopy can provide excellent quantification of common mineral abundances across a broad spectrum of sedimentary samples [1-5]. The infrared spectroscopy procedure utilizes the principle of transitions in a molecule's vibrational and rotational states to detect absorbance by organic bonds and mineral components [6-7].

Although the use of FTIR spectroscopy is constrained by the problem of identifying and interpreting the IR spectra of minerals contained in sediments and soils due to a deficiency of data about characteristic wavenumbers for minerals [8-9], for soil samples, the absorbance of IR bands is determined by the soil's surface solid composition. Therefore, the prediction of chemical properties depends on the soil matrix, such as organic C and total N [10-12]. Variations in soil element concentrations are derived from differences in the composition of the parent material and the fluxes of matter and energy into or from the soil over time [13-14]. Geological controls are more important for soil chemistry in agricultural and grazing land soils than anthropogenic controls [15-16], so variation in soil response is primarily determined by soil mineral and organic composition content [17-18]. Mid-infrared and TXRF spectroscopy both predict soil properties that relate to nutrient buffering capacity, including some exchangeable bases, pH, P sorption capacity, clay and sand content, organic matter content, and basic soil mineralogy fingerprints [19].

Even though X-ray diffraction (XRD) is the industry standard for quantitative mineral analysis, the method's accuracy varies substantially due to differences in sample preparation, sample measurement, and data analysis techniques. Some researchers have shown that several commercially available XRD analyses are generally inaccurate [20]. In particular, commercial laboratories consistently overestimate quartz and underestimate total clay content, which affects the usefulness of soil found at crime scenes in forensic investigations [21] . Studies of artificial mineral mixtures have shown that successful mineral quantification by XRD depends significantly on the operator's choice of sample preparation and method of interpretation rather than on the XRD measurement itself [22]. Moreover, improved resolution, compactness, and scanning range contribute to better quantification outcomes [23].

Fourier transform infrared spectroscopy (FTIR) techniques for studying soil mineralogy use the main carbonate band as a reference for the calculation of the coefficient of extinction [24]. FTIR can identify soil minerals due to the characteristic absorption bands in the middle infrared (IR) range (400 to 4000 cm^{-1}). This method has been used successfully in studies of mineral mixtures and is expected to be superior to XRD because it is sensitive to amorphous materials [25]. In soil sciences, nitrate determination is achieved using methodologies based on infrared spectroscopy [26]. However, signal overlapping and the effects of particle size on FTIR absorbance signals complicate data interpretation. Despite these challenges, it is possible to evaluate relationships between quantitative and qualitative parameters of soil mineral composition using FTIR spectroscopy [27-28]. Different soil types, such as Ultisol and Alfisol, have numerous and distinct indicators that influence the results, making it difficult to generalize the effect of different factors on soil organic matter (SOM) [29-30].

Soil analysis has become routine work for soil management and crop production [31]. However, laboratory-based determination of soil properties is expensive and time-consuming, which is not suitable for precision agriculture. In this study, the transmission FTIR technique for analyzing mineralogy trends in Ultisol and Alfisol soils will be discussed and compared against industry-standard XRD techniques. Ultisols are a significant group of marginal soils developed from claystone and sandstone, extensively found in the upland area of Kendari city. These soils often occur at the knick points of the landscape, where soil creep activates and mobilizes clay along vertical planes in the subsoil. Both Ultisols and Alfisols accumulate clay in their subsoil; however, Ultisols are significantly leached and considerably more weathered than Alfisols, despite their gross morphology being quite similar. Alfisols are more common under forests in cooler, drier climates and younger landscapes where weathering, leaching, and removal of bases are not as extensive. In contrast, Ultisols occur in warmer, wetter, and more stable

landscapes where soils have weathered more and base saturations are consequently lower [32]. The chemical and mineralogical characteristics of their profiles were investigated to better understand the potential of the Ultisols and Alfisols developed in the region.

METHOD

The experiment was conducted in August 2021 in Kendari City, Southeast Sulawesi, Indonesia. The experimental design was a completely randomized block design with three replications, as shown in Figure 1. Alfisol samples were collected from the Mandonga district (3°56'38.2" S, 122°29'54.2" E) labeled as profile 1, Puwatu district (3°57'18.8" S, 122°29'12.0" E) labeled as profile 2, and Puwatu district (3°57'27.3" S, 122°29'00.0" E) labeled as profile 3. Ultisol samples were collected from the Poasia district (4°57'60" S, 122°57'85.32" E) labeled as profile 1, Baruga district (3°57'26.949" S, 122°29'50.02" E) labeled as profile 2, and Poasia district (3°00'54.82" S, 122°46'91.61" E) labeled as profile 3. A total of 60 soil samples of Ultisol and Alfisol were taken from the 0–20, 20–40, 40–80, 80–120, 120–160, and 160–200 cm layers in depth from all profiles (i.e., each profile consists of 10 samples) for chemical and mineralogical characteristics.

Soil samples were air-dried, ground, weighed, sieved through a 2 mm mesh, and stored for subsequent laboratory analysis. Soil pH was measured in aqueous suspensions with a pH meter using a 1:2.5 soil-to-water mixture. The primary chemical properties of the soils were determined using routine methods. Major elements were measured using X-ray fluorescence (XRF) spectrometry performed by the Kendari Assay Laboratory, Indonesia. We determined the selected soil properties and characteristics according to soil survey staff guidelines (U.S. Department of Agriculture, 2004), and total nitrogen was measured by the Kjeldahl method.

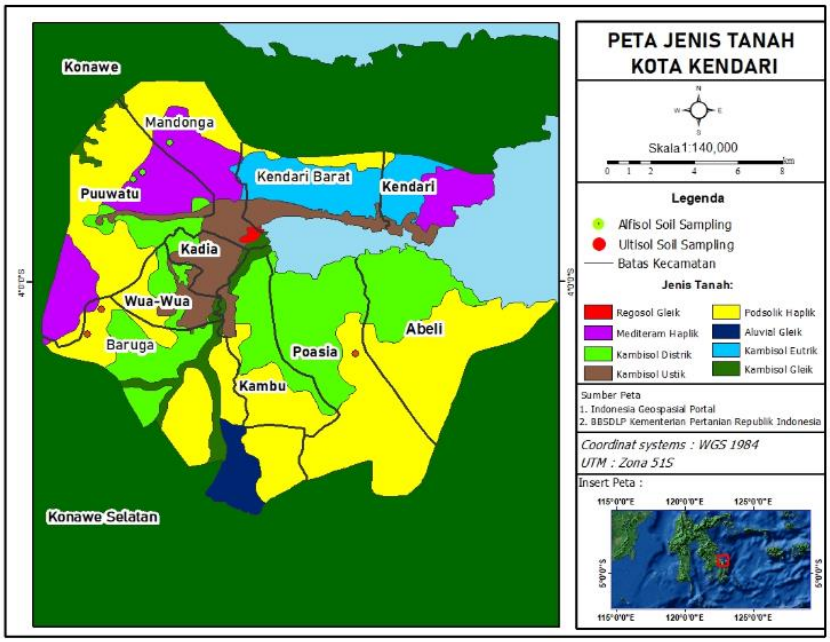

Figure 1. Schematic map of soil types in Kendari City from the Indonesia Geospatial Portal. Sampling sites of Ultisol are marked with rounded red circles and Alfisol marked with rounded Green circles.

RESULTS AND DISCUSSION

The physical properties showed that Ultisol from all profiles had different colors depending on land use and mineral content but were dominated by reddish-yellow to dark brown hues (7.5YR

to 10YR). The color value varied from 3 to 7, and the chroma varied from 4 to 8. Ultisols, composed of granite rich in quartz minerals, typically exhibit a coarse texture, resembling sandy clay. However, Ultisols derived from limestone, andesite rock, and tuff often possess a finer texture, resembling clay and fine clay. Generally, Ultisols feature a moderate to solid structure, characterized by angular lumpy shapes.

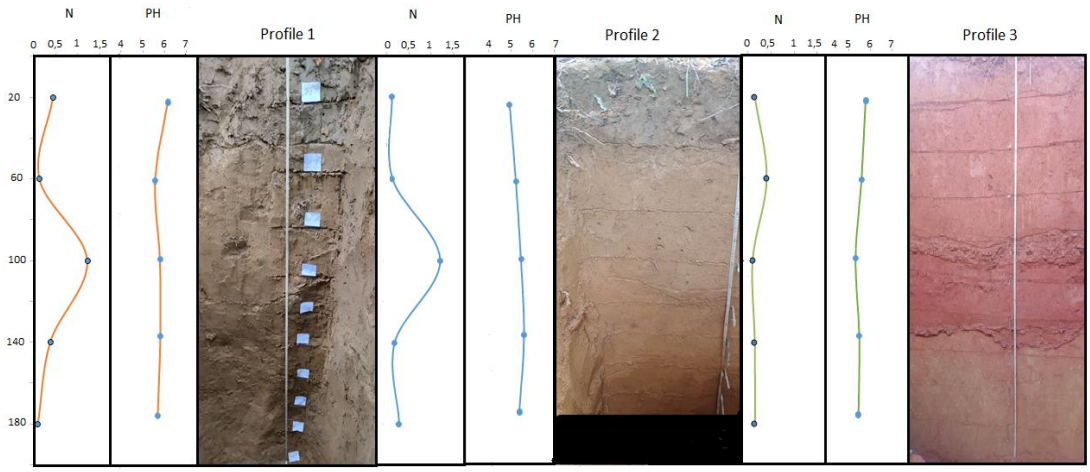

Figure 2. Distribution Pattern of Nitrogen Content and Soil pH for Alfisol Profiles 1, 2, and 3

Alfisols are more common under forests in cooler, drier climates and younger landscapes where weathering, leaching, and removal of bases are not as extensive. In contrast, Ultisols occur in warmer, wetter, and more stable landscapes where soils have weathered more and base saturations are consequently lower. Alfisol from all profiles had different colors depending on land use and mineral content but was dominated by reddish-yellow to dark brown hues (7.5YR to 10YR). The color value varied from 3 to 7, and the chroma varied from 4 to 8. The soil reaction (pH) is slightly acidic in the topsoil, with medium criteria for profiles one and two and low criteria for profile three, ranging from 5.5 to 6.5. The average total nitrogen content of the soil ranges from 0.21% to 0.59% for profile 1, 0.1% to 0.48% for profile two, and 0.1% to 0.39% for profile three, as shown in Figure 3. The upward trend of nitrogen is increasing.

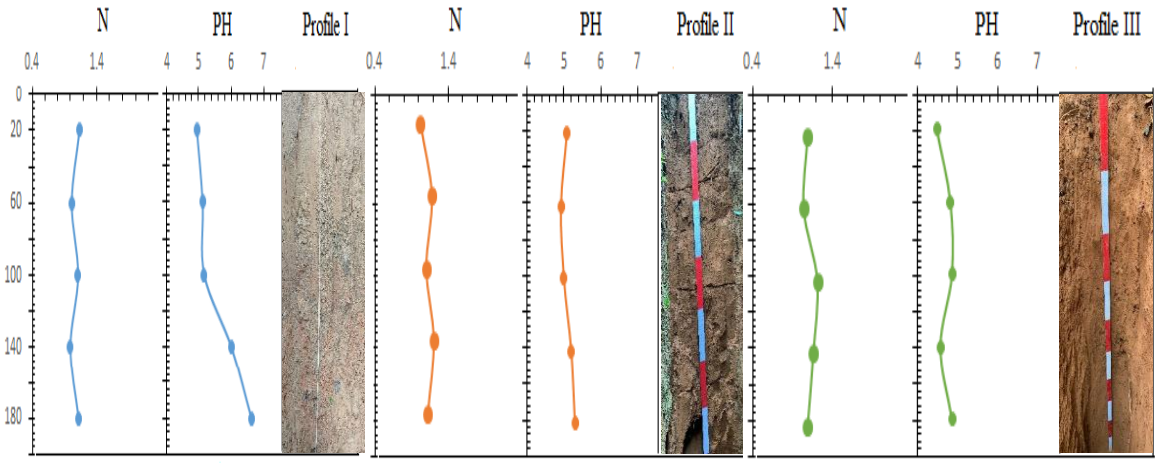

Figure 3. Distribution Pattern of Nitrogen Content and Soil pH for Ultisol Profiles 1, 2, and 3

The chemical element concentrations (Si, Ca, Al, K, Na, Mg, Fe, and S) of Alfisol are shown in Figure 3 and Ultisol in Figure 4 by assigning chemical compositions to each soil layer. These concentrations are then compared against the major elemental concentrations of Alfisol to

obtain specific patterns. The differing patterns assess conformance between the measured elemental concentrations of the two soil types and recognize natural variability in the chemical compositions of certain sedimentary minerals.

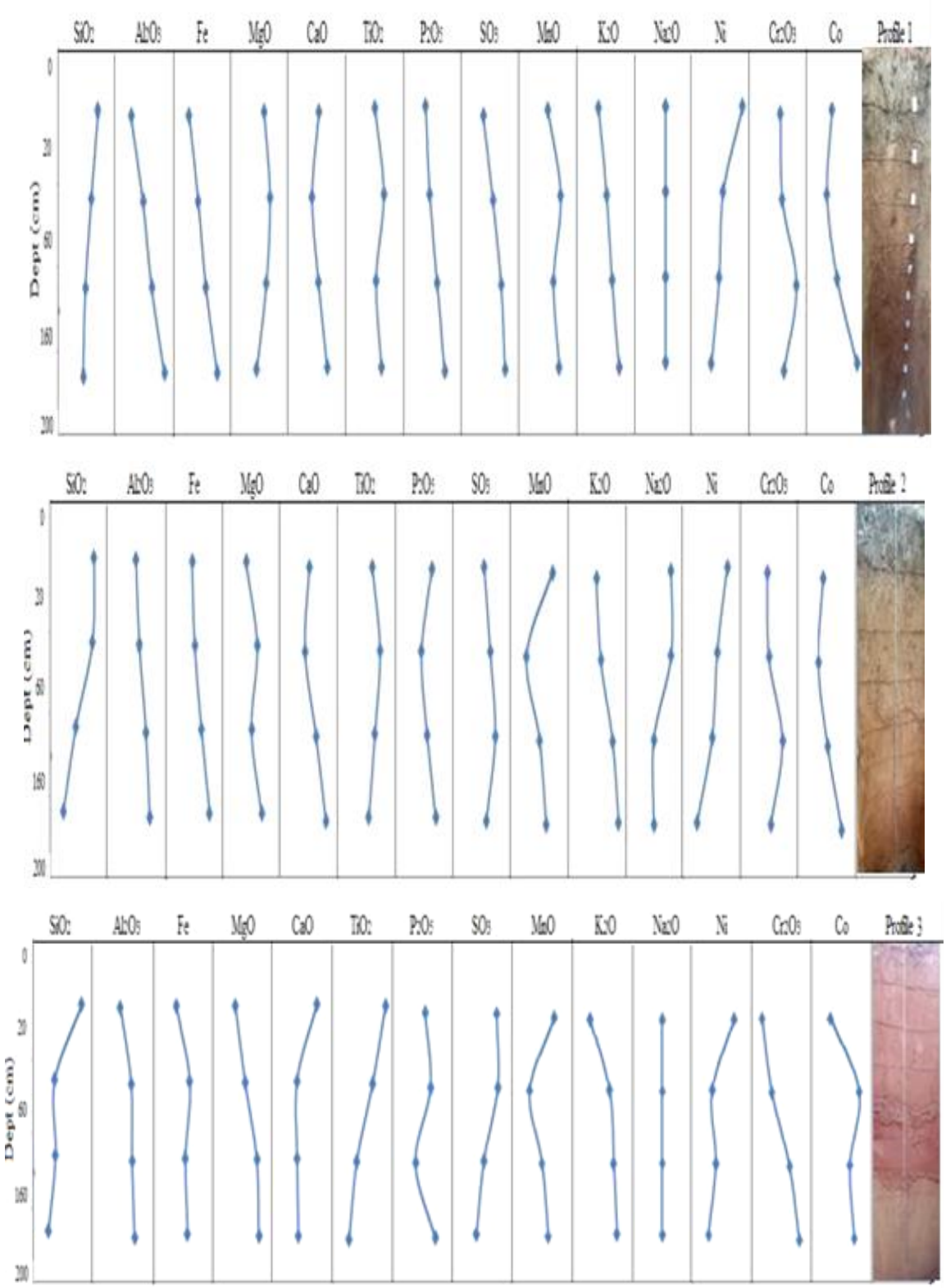

Figure 4. Normalized Chemical Element Concentrations of Alfisol as a Function of Depth for the Three Profiles

Ultisols, composed of granite rich in quartz minerals, typically exhibit a coarse texture, resembling sandy clay. However, Ultisols derived from limestone, andesite rock, and tuff often possess a finer texture, resembling clay and fine clay. Generally, Ultisols feature a moderate to solid structure, characterized by angular lumpy shapes.

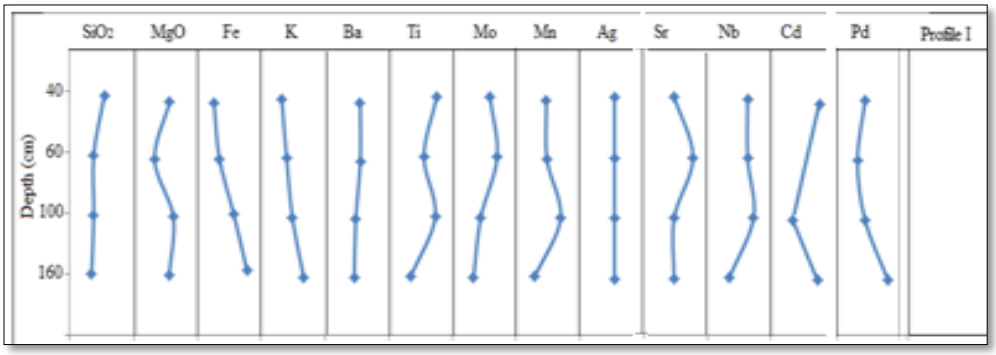

(a) Profile 1

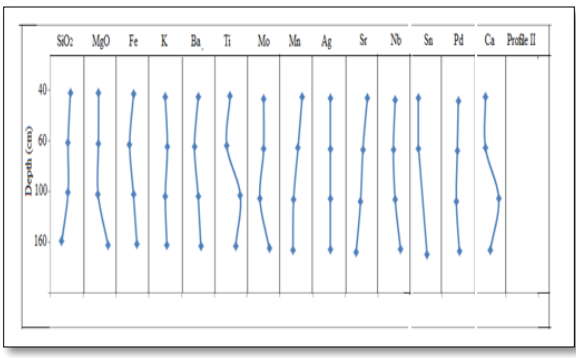

(b) Profile 2

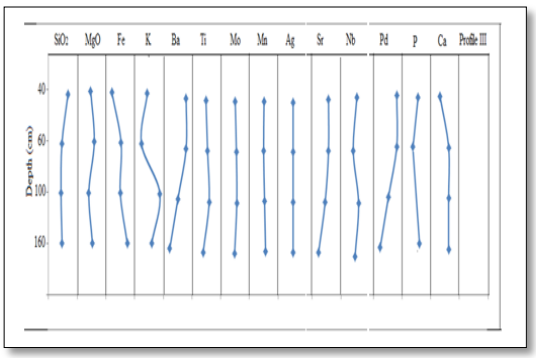

(c) Profile 3

Figure 5. Normalized Chemical Element Concentrations of Ultisol as a Function of Depth for the Three Profiles

The chemical analysis of bulk concentrations of major mineral-forming elements (Si, Al, Ca, Mg, K, Na, Fe, Ti, Mn) in all samples was conducted using X-ray fluorescence spectrometry (XRF). Figures 3 and 4 compare the measured major-element concentrations at different soil depths for each profile, showing a wide range of compositions. The error in the XRF measurement is 0.1 wt% for the major elements. The XRF analysis identified fourteen elements present in all profiles, both Ultisol and Alfisol, including major elements such as Si, Al, Fe, Mg, Ti, Ca, S, Na, K, P, Mn, Ni, Co, and Cr, each with a specific pattern.

SiO_2 is the most abundant element in both Ultisol and Alfisol profiles. In Alfisol, its content ranges from 58.23% to 72.37% in Profile 1, from 59.5% to 67.7% in Profile 2, and from 59.91% to 69.35% in Profile 3. Al_2O_3 follows, ranging from 8.52% to 16.2% in Profile 1, from 11.28% to 16.32% in Profile 2, and from 13.28% to 15.15% in Profile 3. Iron (Fe) and magnesium (Mg) contents range from 1.89% to 5.24% and 0.54% to 0.81%, respectively, in Profile 1; from 2.6% to 4.5% and 0.45% to 0.64% in Profile 2; and from 3.1% to 5.38% and 0.37% to 0.52% in Profile 3. In all Alfisol profiles, titanium (Ti) ranges from 0.61% to 1.0%, calcium (Ca) from 0.03% to 0.3%, and phosphorus (P) from 0.03% to 0.25%. Minor elements with concentrations below 0.1% also exhibit specific patterns, as shown in Figure 4.

Ultisol profiles show variability in elemental concentrations. SiO_2 ranges from 57.2% to 79.75%, Fe from 1.0% to 6.17%, Al_2O_3 from 3.34% to 6.78%, K from 0.3% to 2.1%, MgO from 0.88% to 1.34%, and Ba from 0.32% to 0.4%. Minor elements such as Mn, Ar, Sr, P, Ca, and Mo follow specific patterns, as shown in Figure 5.

Significant trends emerge when comparing the chemical composition of Alfisol and Ultisol profiles, indicating distinct elemental distribution patterns.s. The Si trend increases upward, while Al, Fe, and Mg oxide trends increase downward across all profiles. Conversely, total P and K, essential for soil fertility, show a downward trend with depth, indicating an abundance of nutrients in the topsoil. The presence of elements such as nickel (Ni), chromium (Cr), and cobalt (Co) is particularly important for soil properties due to their high magnetic susceptibility and economic valueIt is essential to note that not all minerals common to sedimentary formations have fixed elemental compositions; their major cation abundances can naturally vary within a limited range constrained by their crystallographic structure. Clay minerals, particularly sedimentary illites, smectites (montmorillonite), and chlorites, are common minerals that show chemical compositional variability [12]. Commercial XRD laboratories commonly analyze mineralogy using XRD techniques, shown in Figure 5 and Figure 6

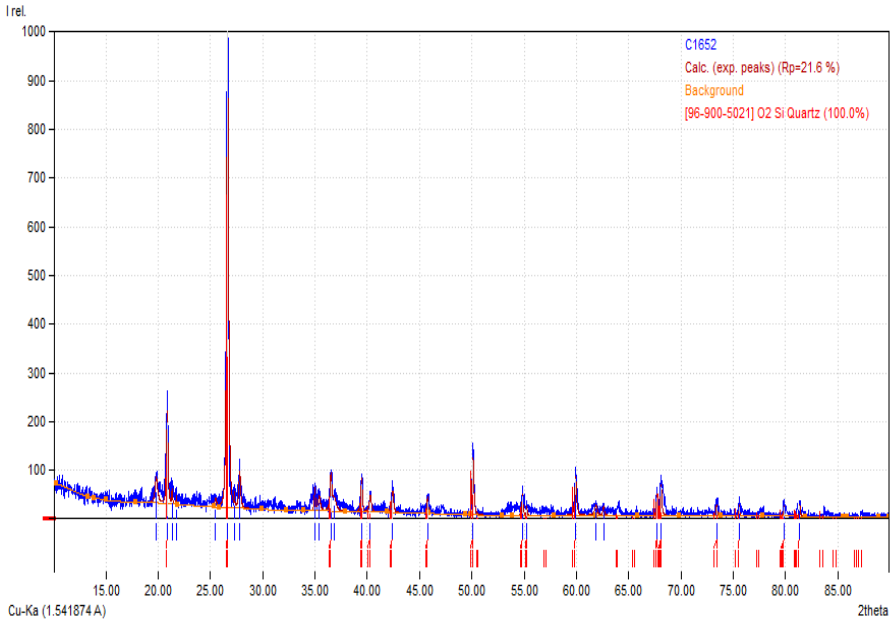

(a) Profile 1

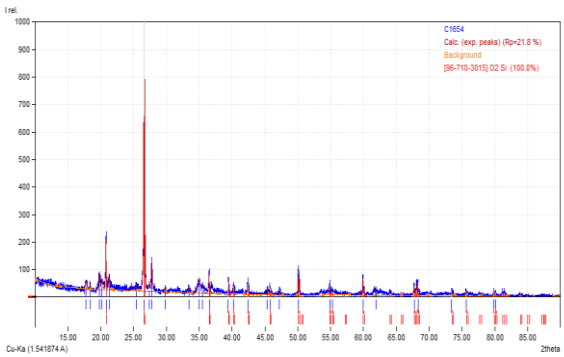

(b) Profile 2

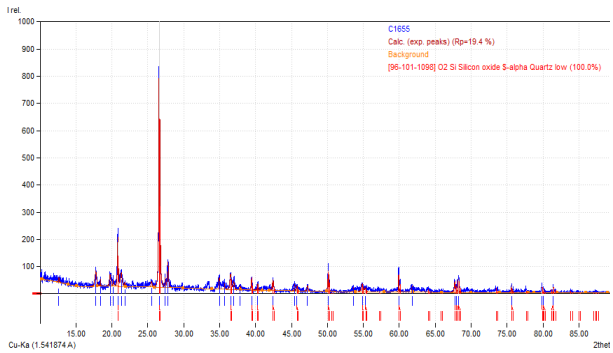

(c) Profile 3

Figure 6. XRD analysis of Alfisol for the Three Profiles

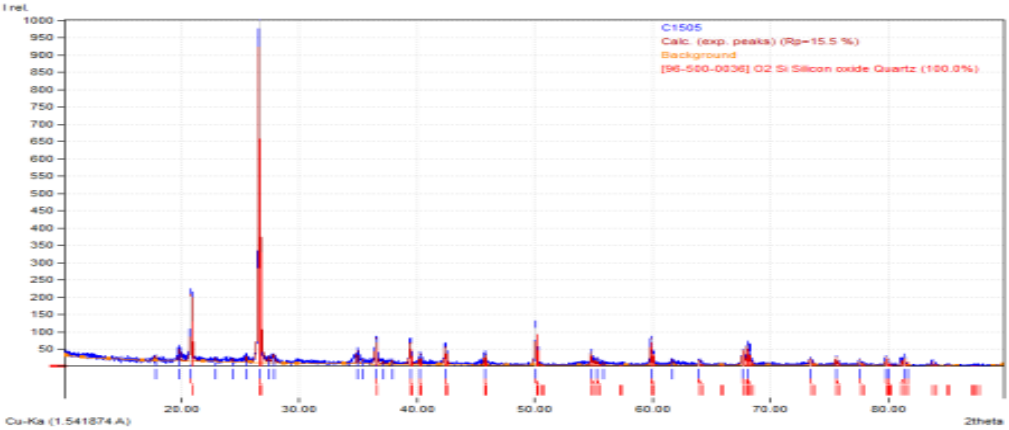

(a) Profile 1

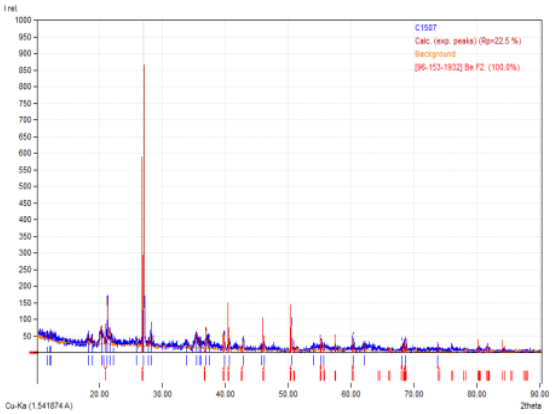

(b) Profile 2

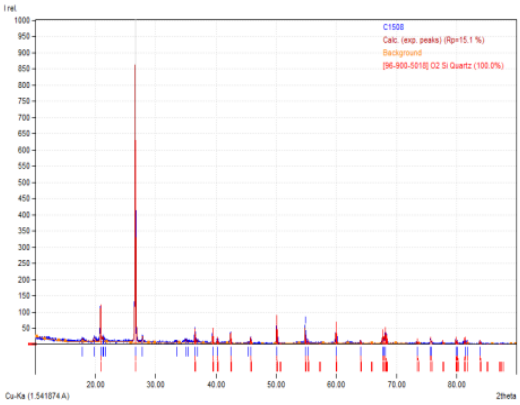

(c) Profile 3

Figure 7. XRD analysis of Ultisol for the Three Profiles

As demonstrated below, such compositional variability can lead to a range of possible elemental reconstructions for a given set of mineralogy. However, this variability alone is not sufficient to explain the discrepancies observed between mineralogy and bulk chemical compositions or between two sets of mineralogy results on the same set of samples. The diffraction pattern graphics of topsoil from the three profiles are presented in Figures 5 and 6. All profiles identified 100% silicon oxide quartz (SiO2) in the low phase with a trigonal (hexagonal axes) crystal system.

Identification of an IR spectrum of geological samples is a complicated process because sediments are a mixture of different minerals, and the fingerprint zone of the spectrum can overlap. The most common minerals in soils include various clays (e.g., kaolinite), calcites, and different morphological forms of silica. The study of soils using FTIR spectroscopy tools with an infrared spectrum range of 400–4000 cm -1can be approximately performed for both Ultisol and Alfisol across three profiles (i.e., profile-1, profile-2, and profile-3). The nature of the group frequency variation at different depths (i.e., 20 cm, 40 cm, 80 cm, 120 cm, 160 cm, and 200 cm) is generally determined by fundamental vibrations. The suitable soil components and the characterization of soil minerals and organic matter from the three profiles were analyzed by infrared spectroscopy, as shown in Figure 6.

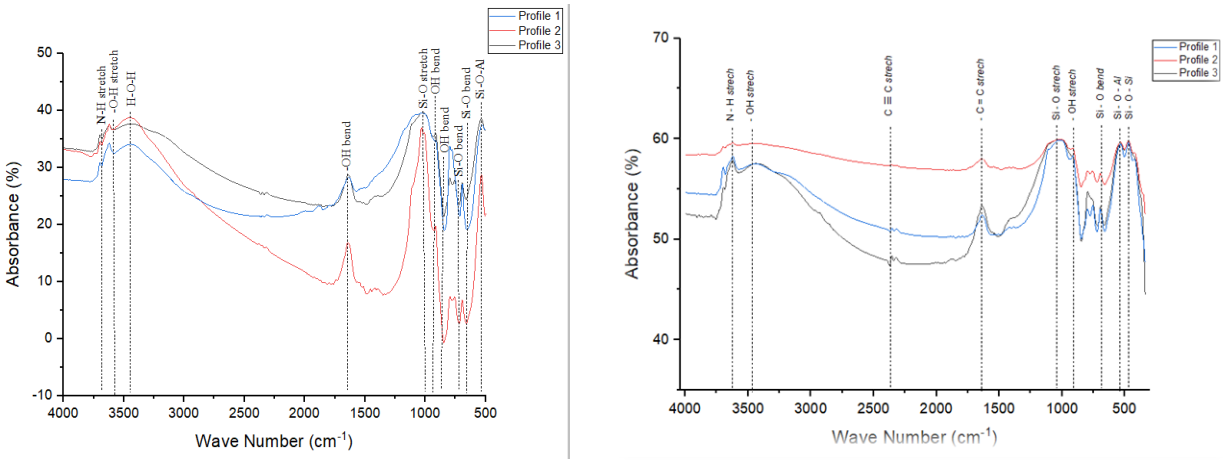

Figure 8. Description of Wave Absorbtion in 20 cm (top soil): left ultisol and right alfisol

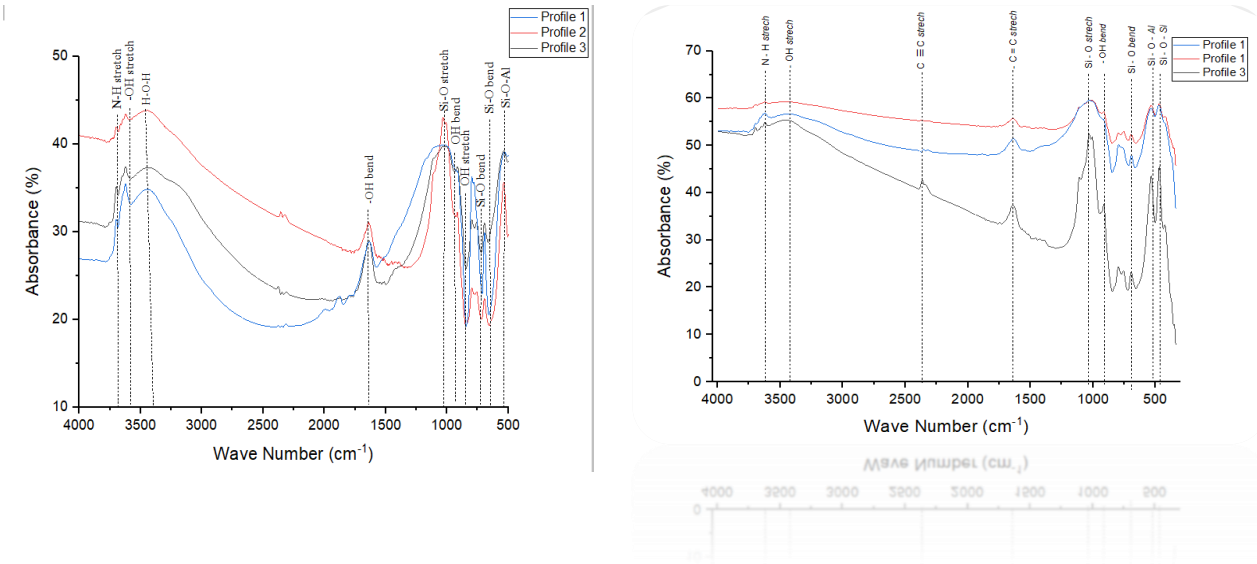

Figure 9. Description of Wave Absorbtion in 40 cm: left ultisol and right alfisol

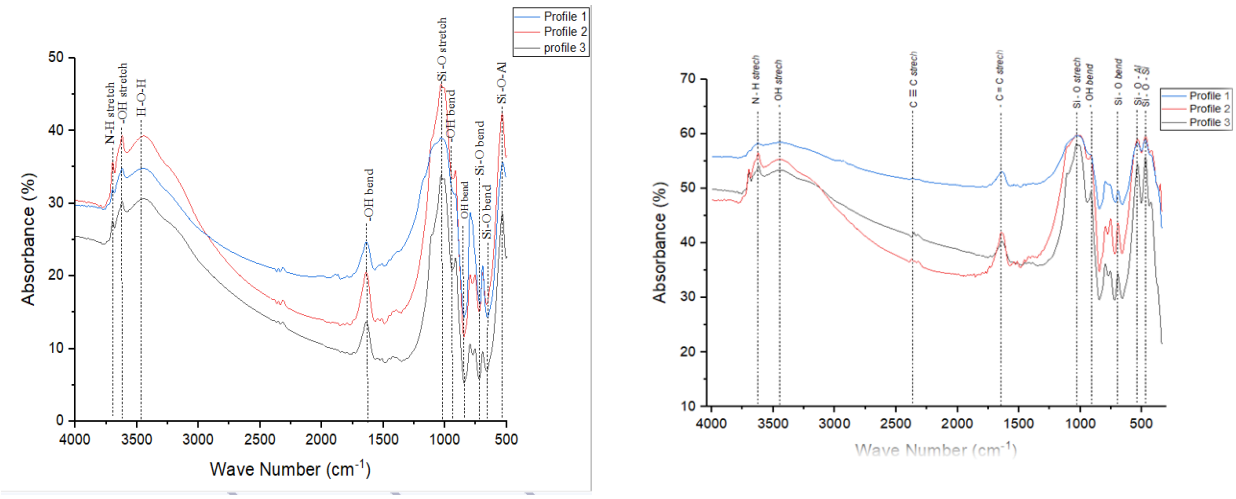

Figure 10. Description of Wave Absorbtion in 80 cm: left ultisol and right alfisol

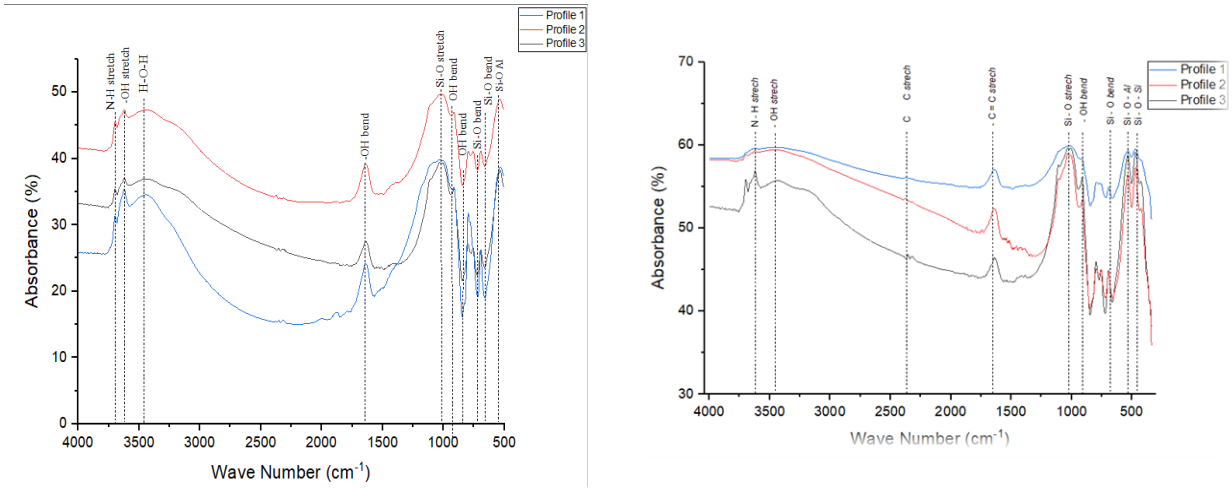

Figure 11. Description of Wave Absorbtion in 120 cm : left ultisol and right alfisol

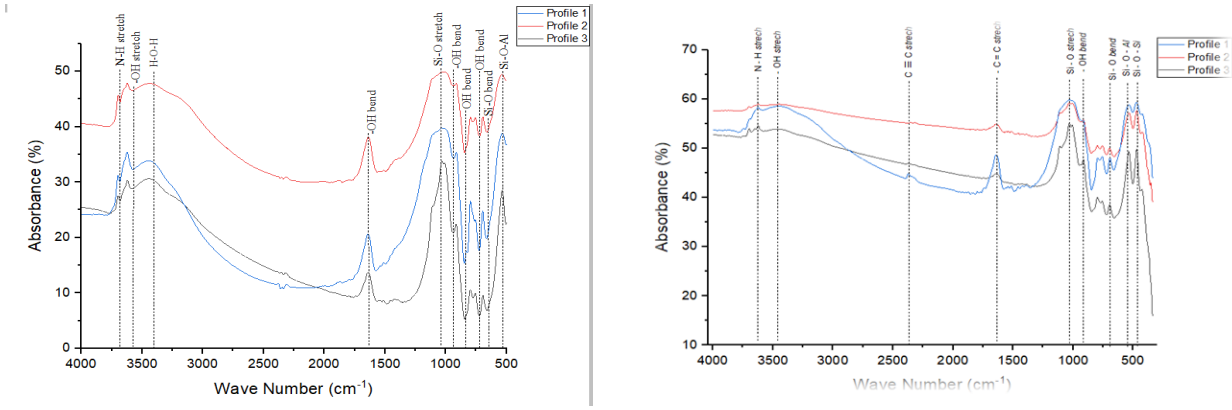

Figure 12. Description of Wave Absorbtion in 160 cm : left ultisol and right alfisol

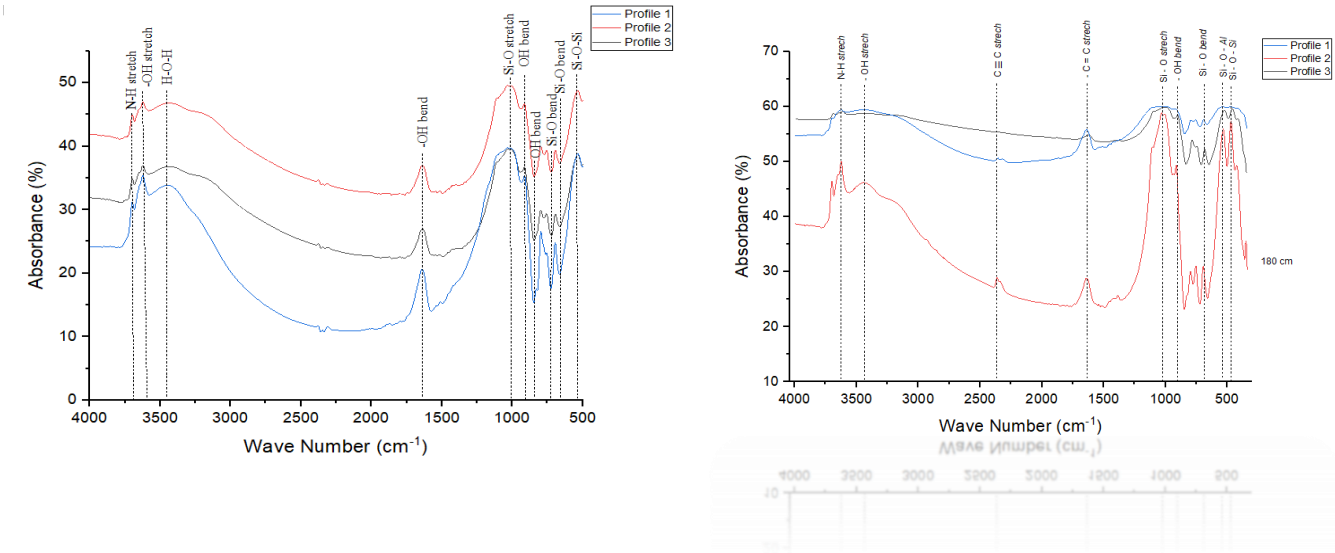

Figure 13. Description of Wave Absorbtion in 200 cm: left ultisol and right alfisol

A broader band can be observed in transmittance spectra in the region encompassing the following absorption bands: 3620 cm^{-1} (N-H streching); 3480 cm^{-1} (O–H stretching of various functional groups); 2925 and 2850 cm^{-1} (aliphatic C–H group stretching); 1720 cm^{-1} (C=O

stretching of carboxyl groups); 1650 cm^{-1} (aromatic C=C stretching and COO– symmetric stretching); 1508 cm^{-1} (amide II band); 1450 cm^{-1} (aliphatic C–H deformation); 1424 cm^{-1} (amide III band); 1130 cm^{-1} (C–OH deformation of aliphatic OH); a broad band at 1225 cm^{-1} (C–O stretching and O–H deformation of carboxyl and C–O stretching of aryl ethers and phenols); and 1030 cm^{-1} (C–O stretching of polysaccharides). However, the fingerprint absorptions (500–1000 cm^{-1}) are significantly different, which implies that the general structure of substituent groups attached significantly varied. The absorption of the aliphatic group (approximately 2900 cm^{-1}) may have a strong capability for water repellence. More specific assignments of absorption bands are shown in Table 1and Tabel 2.

The height of the aliphatic band (2905 cm^{-1}) for Alfisol is higher than and Ultisol and the height of the carboxyl band (1711 cm cm^{-1}) for Alfisol and Ultisol, but, the ratios value of aliphatic to carboxyl bands for Alfisol and Ultisol relatifly the same. Thus, water repellence of Alfisol and Ultisol. The higher carboxyl group absorption in Alfisol compared to its aliphatic absorption suggests that Alfisol is more humic than Ultisol.

Clays have diagnostic IR absorption bands between approximately 3200 and 3600 cm^{-1} associated with stretching modes of water and hydroxyls. Molecular water can interfere with the interpretation of these diagnostic IR absorption bands. Additionally, the absorbance bands correspond to various organic functional groups, including alcohol O-H stretching in the strong broad range (3420-3440 cm^{-1}), aliphatic primary amine N-H stretching at (3697-3620 cm^{-1}), amine and cyclic alkene in the (1665-1630 cm^{-1}) region due to N-H bending and C=C stretching vibration, and aliphatic C-H bending at 1872 cm^{-1} Although there is overlapping low absorbance intensity of organic functional groups and dominant absorbance of mineral components, particularly Si-O stretching, which occurs in the range 1100-800 cm^{-1}, making interpretation of this band difficult.

Table 1. Descrpition Wave Absorbtion of Alfisol in Profile 1

	Depth (cm)						**Functional Groups**
	20 cm	**40 cm**	**80 cm**	**120 cm**	**160 cm**	**200 cm**	
Wave number (cm-1)	3695	3695	3695	3695	3696	3697	OH streching
	3622,32	3622,32	3624,25	3622,32	3622,32	3622,32	N-H streching
	1029,99	1029,99	1029,99	1031,92	1031,92	1031,92	Si-O streching
	918,12	918,12	918,12	918,12	918,12	916,19	OH bending
	797	797	797	797	795	794	Si-O stretching
	694,37	694,37	694,37	694,37	694,37	694,37	Si-O bending
	536,21	536,21	536,21	534,28	534,28	536,21	Si-O-Al bending
	472	472,56	472,56	472,56	472,56	474,49	Si-O-Al bending

In the Alfisol absorbance spectrum, all profiles show that the average absorbance varies with depth (i.e., 20 cm, 40 cm, 80 cm, 120 cm, 160 cm, and 200 cm). The OH stretching and bending occur at 3695 cm $^{-1}$ and 3622 cm $^{-1}$ (3700-3620 cm $^{-1}$ band) and at 912 cm $^{-1}$ (920-916 cm $^{-1}$ band). Silicate Si-O asymmetric stretching is observed at 1030 cm $^{-1}$ (1090-1030 cm $^{-1}$ Si-O symmetric stretching at 790 cm $^{-1}$ (790- cm^{-1} band), and Si-O bending at 693 cm $^{-1}$ (695-690 cm $^{-1}$). Specific absorption fingerprints are sensitive enough to distinguish Si-O-Al bending and Si-O-Si bending, enabling identification of the phyllosilicate structural class. According to the position of the main absorption band for minerals that commonly interfere in crystalline quartz analysis[12], the aforementioned spectra with the analytical peak indicate the presence of the kaolinite mineral type. Kaolinite is a 1:1 layer silicate that exhibits two or three OH stretching absorptions. A high concentration of Si, Al, Fe, and Mg contents in the Alfisol profile, as shown

in Figure 1, indicates a triumvirate of Si-O absorbance at 1120-950 cm $^{-1}$, attributed to hydrothermally, specifically kaolinite (Al2Si2O5(OH)4). Kaolinite have the specific vibrational modes on band from 3695 cm^{-1}to 3650 cm-1 that indentify as OH Stretching, band 910-915 cm^{-1} as Al-OH Bending and band 1000-1100 cm^{-1}.

On the other hand, the absorbance spectrum in Ultisol profile one in the Poasia district shows OH stretching occurring at 3622 cm $^{-1}$, where the 2:1 layer silicates contain a single OH stretching band (3700-3620 cm $^{-1}$) shown in all layers of depth, attributed to OH coordinated with octahedral cations. High Al, Fe, and Mg contents of soil, with these patterns increasing with depth as presented in Figure 8, indicate Al2OH vibration (3620 cm^{-1} and 916 cm $^{-1}$ and FeAlOH (890-910 cm $^{-1}$) and MgAlOH (850 cm^{-1}) in montmorillonite.

Table 2. Descrpition Wave Absorbtion of Ultisol in Profile 1

	Depth (cm)						**Functional Groups**
	20	**40**	**80**	**120**	**160**	**200**	
Wave number (cm^{-1})	3620,39	3622,32	3620,39	3620,39	3620,39	3622,32	N-H streching
	3441,01	3441,01	3442,94	3421,72	3446,79	3431,36	OH streching
	2353,16	2353,16	2355,08	2355,08	2374,37	2374,37	C ≡ C streching
	1639,49	1639,49	1641,42	1639,49	1643,35	1643,28	C = C streching
	1029,99	1029,99	1031,92	1031,92	1029,99	1031,92	Si-O streching
	916	918	916	916	916	916	OH bending
	845	850	850	850	845	855	OH bending
	694,37	694,37	694,37	696,30	696,30	696,30	Si-O bending
	534,28	536,21	536,21	536,21	534,28	536,21	Si-O-Al bending
	470,64	472,56	470,63	470,63	470,63	470,63	Si-O-Al bending

On the other hand, profiles two and three in the Baruga district fit the kaolinite absorption peaks at wavenumbers 3694, 3620, 1030, 1009, 912, 792, 756, 694, 536, 470, and 425 cm $^{-1}$. It appears that using the FTIR analytical approach, we can investigate the soil minerals in both Alfisol and Ultisol for all profiles. However, understanding the influence of clay swelling on the soil type and the physical breakdown of mineral soil was also employed using micro-ATR spectroscopy. Montmorillonite have 2:1 layer structure (one octahedral sheet sandwiched between two tetrahedral sheets) can absorb water between layers with chemical formula (Na,Ca)0.33(Al,Mg)2Si4O10(OH)2•nH2O. In the Ultisoll absorbance, all profiles show spectrum OH Stretching in Broad band around 3400-3500 cm^{-1}due to water absorption, Al-OH Bending in 845 cm^{-1} (Mg-OH stretching), Si-O Stretching, 1000-1050 cm^{-1} and H2O deformation in 1630 cm^{-1}.

CONCLUSION

Alfisols with a pH range 5.5 to 6.5 (less acidic), are well-suited for growing a wide range of crops with high concentration of Si, Al, Fe, and Mg contents in all layers. FTIR spectroscopy analysis showed progressive kaolinization in all Alfisol samples. In contrast, Ultisol profiles expressed montmorillonite, more acidic, so it require more intensive management for agriculture. Significant trends of the chemical elements between Alfisol and Ultisol profiles, indicating unique patterns, Si trend increases upward, while Al, Fe, and Mg oxide trends

increase downward across all profiles. Conversely, total P and K, essential for soil fertility, show a downward trend with depth, indicating an abundance of nutrients in the topsoil.

REFERENCES

1 Nieto, J. L. 1978. Infrared determination of quartz, Kaolin, corundum, silicon carbide and orthoclase in respirable dust from grinding wheels. *Analyst*, *103*(1223), 128-133.

2 Craddock, P. R., Herron, M. M., & Herron, S. L. 2017. Comparison of quantitative mineral analysis by X-ray diffraction and Fourier transform infrared spectroscopy. *Journal of Sedimentary Research*, *87*(6), 630-652.

3 Chukanov, N. V., & Chervonnyi, A. D. 2016. *Infrared spectroscopy of minerals and related compounds*. Springer.

4 Sánchez-Sánchez, A., Cerdán, M., Jordá, J. D., Amat, B., & Cortina, J. 2019. Characterization of soil mineralogy by FTIR: Application to the analysis of mineralogical changes in soils affected by vegetation patches. *Plant and Soil*, *439*, 447-458.

5 Zornoza, R., Guerrero, C., Mataix-Solera, J., Scow, K. M., Arcenegui, V., & Mataix-Beneyto, J. 2008. Near infrared spectroscopy for determination of various physical, chemical and biochemical properties in Mediterranean soils. *Soil Biology and Biochemistry*, *40*(7), 1923-1930.

6 Parikh, S. J., Goyne, K. W., Margenot, A. J., Mukome, F. N., & Calderón, F. J. 2014. Soil chemical insights provided through vibrational spectroscopy. *Advances in agronomy*, *126*, 1-148.

7 Parikh, S. J., Goyne, K. W., Margenot, A. J., Mukome, F. N., & Calderón, F. J. 2014. Soil chemical insights provided through vibrational spectroscopy. *Advances in agronomy*, *126*, 1-148.

8 Tkachenko, Y., & Niedzielski, P. 2022. FTIR as a method for qualitative assessment of solid samples in geochemical research: a review. *Molecules*, *27*(24), 8846.

9 Robertson, A. J., Hill, H. R., & Main, A. M. 2013. Analysis of Soil in the Field using portable FTIR. In *International Workshop on Soil Spectroscopy: The Present and Future of Soil Monitoring*.

10 Šimon, T. 2007. Characterisation of soil organic matter in long-term fallow experiment with respect to the soil hydrophobicity and wettability.

11 Haberhauer, G., Feigl, B., Gerzabek, M. H., & Cerri, C. 2000. FT-IR spectroscopy of organic matter in tropical soils: changes induced through deforestation. *Applied Spectroscopy*, *54*(2), 221-224.

12 Ojima, J. 2003. Determining of crystalline silica in respirable dust samples by infrared spectrophotometry in the presence of interferences. *Journal of Occupational Health*, *45*(2), 94-103.

13 Margenot, A. J., Calderón, F. J., Goyne, K. W., Dmukome, F. N., & Parikh, S. J. 2016. IR spectroscopy, soil analysis applications. In *Encyclopedia of spectroscopy and spectrometry* (pp. 448-454). Elsevier.

14 Madari, B. E., Reeves III, J. B., Machado, P. L., Guimarães, C. M., Torres, E., & McCarty, G. W. 2006. Mid-and near-infrared spectroscopic assessment of soil compositional parameters and structural indices in two Ferralsols. *Geoderma*, *136*(1-2), 245-259.

15 Saaltink, R., Griffioen, J., Mol, G., Birke, M., & GEMAS Project Team. 2014. Geogenic and agricultural controls on the geochemical composition of European agricultural soils. *Journal of Soils and Sediments*, *14*, 121-137.

16 Reeves, J. B., McCarty, G. W., & Reeves, V. B. 2001. Mid-infrared diffuse reflectance spectroscopy for the quantitative analysis of agricultural soils. *Journal of agricultural and food chemistry*, *49*(2), 766-772.

17 Margenot, A. J., Calderón, F. J., Bowles, T. M., Parikh, S. J., & Jackson, L. E. 2015. Soil organic matter functional group composition in relation to organic carbon, nitrogen, and phosphorus fractions in organically managed tomato fields. *Soil Science Society of America Journal*, *79*(3), 772-782.

18 Achat, D. L., Pousse, N., Nicolas, M., Brédoire, F., & Augusto, L. 2016. Soil properties controlling inorganic phosphorus availability: general results from a national forest network and a global compilation of the literature. *Biogeochemistry*, *127*, 255-272.

19 Towett, E. K., Shepherd, K. D., Sila, A., Aynekulu, E., & Cadisch, G. 2015. Mid-infrared and total x-ray fluorescence spectroscopy complementarity for assessment of soil properties. *Soil Science Society of America Journal*, *79*(5), 1375-1385.

20 Cannane, N. O. A., Rajendran, M., & Selvaraju, R. 2014. Mineralogical identification on polluted soils using XRD method. *J Environ Nanotechnol*, *3*, 23-29.

21 Willms, M., Drake, R., Leftwich, K., DeLuca, D., & Jasra, S. K. 2017. X-Ray diffraction comparison of Windsor area soil mineralogy for forensic investigations. *Journal of Emerging Forensic Sciences Research*, *2*(1), 65-74.

22 Zhang, Z., Sheng, Q., Zhao, M., Zhong, J., He, N., Li, R., ... & Zhang, J. 2021. Analysis of soil clay mineral in terrestrial ecosystem using X-ray diffraction spectroscopy. *Spectroscopy Letters*, *54*(1), 65-71.

23 Rocha, D. R., Barber, X., Jordán-Vidal, M. M., Urbano, A., Melquiades, F. L., Thomaz, E. L., & Mataix-Solera, J. 2022. Multivariate Analysis with XRD Data as a Fingerprinting Technique to Study Burned Soils. *Minerals*, *12*(11), 1402.

24 Jordá, J. D., Jordán, M. M., Ibanco-Cañete, R., Montero, M. A., Reyes-Labarta, J. A., Sánchez, A., & Cerdán, M. 2015. Mineralogical analysis of ceramic tiles by FTIR: A quantitative attempt. *Applied Clay Science*, *115*, 1-8.

25 Xu Z., Cornilsen B.C., Popko D.C., Wei B., Pennington W.D., Wood J.R. 2001. Quantitative Mineral Analysis by FTIR Spectroscopy. *Internet J. Vib. Spectrosc*, *5*, 1–11. Online: www.ijvs.com

26 Linker, R., Weiner, M., Shmulevich, I., & Shaviv, A. 2006. Nitrate determination in soil pastes using attenuated total reflectance mid-infrared spectroscopy: Improved accuracy via soil identification. *Biosystems Engineering*, *94*(1), 111-118.

27 Krivoshein, P. K., Volkov, D. S., Rogova, O. B., & Proskurnin, M. A. 2020. FTIR photoacoustic spectroscopy for identification and assessment of soil components: Chernozems and their size fractions. *Photoacoustics*, *18*, 100162.

28 Du, C., Zhou, J., Wang, H., Chen, X., Zhu, A., & Zhang, J. 2009. Determination of soil properties using Fourier transform mid-infrared photoacoustic spectroscopy. *Vibrational Spectroscopy*, *49*(1), 32-37.

29 Ananthapadmanabha, A. L., Shankar, R., & Sandeep, K. 2014. Rock magnetic properties of lateritic soil profiles from southern India: Evidence for pedogenic processes. *Journal of Applied Geophysics*, *111*, 203-210.

30 Osanai, Y., Knox, O., Nachimuthu, G., & Wilson, B. 2020. Contrasting agricultural management effects on soil organic carbon dynamics between topsoil and subsoil. *Soil Research*, *59*(1), 24-33.

31 Cantarella, H., Quaggio, J. A., van Raij, B., & de Abreu, M. F. 2006. Variability of soil analysis in commercial laboratories: implications for lime and fertilizer recommendations. *Communications in Soil Science and Plant Analysis*, *37*(15-20), 2213-2225.

32 Fiantis, D. 2017. *Morfology dan Klasifikasi Tanah*. Universitas Andalas.